Control of the Subinclusion Microstructure in HDPE/PS/PMMA Ternary Blends

Joël Reignier and Basil D. Favis*

CRASP, Department of Chemical Eng., Ecole Polytechnique, Montreal, QC H3C 3A7 Canada

Received November 19, 1999; Revised Manuscript Received June 8, 2000

ABSTRACT: Various ternary blends of HDPE, PS, and PMMA were prepared in one step using a Brabender mixer. When HDPE is the major component, as in this case, the morphology consists of a HDPE matrix, a PS dispersed phase and PMMA subinclusions within the dispersed PS, as predicted by the spreading coefficients. SEM observation and quantitative characterization were used to show that this complex morphology occurs within the first minutes of mixing and remains stable thereafter. Furthermore, it is shown quantitatively that all the PMMA is present in subinclusion form. It is possible to manipulate the dispersed phase internal structure from small PMMA subinclusions dispersed in a larger PS particle to a PS/PMMA core−shell structure upon decreasing the PS/PMMA composition ratio. Coalescence of composite droplets was also investigated. Upon annealing, these systems clearly experience a dual coalescence process: composite droplet/composite droplet coalescence and coalescence between dispersed subinclusion particles. Although some particle size increase is observed, the main effect of static coalescence is the transition from dispersed subinclusions to a core−shell structure at long times. It is shown that dynamic coalescence is controlled by the thickness of the shell layer. Morphological changes of the composite droplet size were also measured and explained in terms of interfacial tension and viscosity reductions. It is demonstrated that the composite droplet size is controlled by the outer shell thickness.

1. Introduction

In the past 20 years, research into polymer blends has increased significantly since it is a route to obtain new high performance organic materials without synthesizing totally new polymers. Generally, these systems are composed of two immiscible polymers with or without a compatibilizer and display a classical matrix/dispersed phase morphology which depends on the composition and viscoelastic properties of the individual components. Recently, there has been interest in multiphase polymer blends which exhibit another morphology, the composite droplet morphology. This term is used to describe a droplet in droplet type blend morphology (the term subinclusion is also used). Since the mechanical properties of multiphase blends are influenced for the most part by their phase morphologies and the interfacial chemistry, the understanding and control of the phase microstructure of composite droplet multiphase blends is very important.

The well-known high impact polystyrene (HIPS) possesses a salami-type microstructure which is generated during polymerization and is related to styrene/butadiene miscibility.[1,2] The formation of subinclusion morphologies via melt mixing, however, has not been studied extensively and for a number of years was reported as a curious observation. In some cases, subinclusion formation was related to the minimization of surface free energy (Berger et al.,[3] Van Oene[4]) or to the entrapment of subinclusions in a more viscous phase near the phase inversion region (Favis and Chalifoux[5]).

The most recent work has been concerned with the formation and control of these structures in immiscible as-polymerized systems using melt processing equipment. Favis et al.[6] showed that a composite droplet structure could be generated for a 50/50% incompatible binary blend of polypropylene (PP) and polycarbonate (PC) after melt blending near the phase inversion region, as well as at lower PC concentration (volume fraction = 0.25) by selectively imposing phase inversion and controlling the time of mixing. That system consisted of a PP matrix and PP subinclusions within the more viscous PC dispersed phase. For the PP/PC system, increasing the viscosity of the dispersed phase (PC) was found to improve the retention of subinclusions with mixing time. In the case of a polyamide (PA)/polyethylene (PE) copolymer system, an interfacial reaction between subinclusions and the dispersed phase resulted in a complete stabilization and high retention of the subinclusions, even for a relatively low dispersed phase viscosity and long mixing times.

Several authors have reported on the spontaneous development of the composite droplet morphology. On the basis of interfacial energy differences between the blend components, Torza and Mason[7] predicted a composite droplet morphology for two immiscible liquid drops suspended in a third immiscible liquid. Hobbs et al.[8] rewrote the Harkin's equation for a system in which two dissimilar polymers are dispersed within a third by substituting the appropriate interfacial tensions for the surface tensions values

$$\lambda_{31} = \sigma_{12} - \sigma_{32} - \sigma_{13} \quad (1)$$

where σ_{12}, σ_{32}, and σ_{13} are the interfacial tensions for each component pair, and λ_{31} is defined as the spreading coefficient for component 3 (shell) to encapsulate component 1 (core). The index 2 refers to the matrix. λ_{31} must be positive for component 1 to be encapsulated by component 3. If λ_{31} and λ_{13} are negative, phases 1 and 3 will tend to be dispersed separately in the matrix of 2. Furthermore, in the particular case where λ_{21} is also

* To whom correspondence should be addressed.

10.1021/ma991954g CCC: $19.00 © 2000 American Chemical Society
Published on Web 08/26/2000

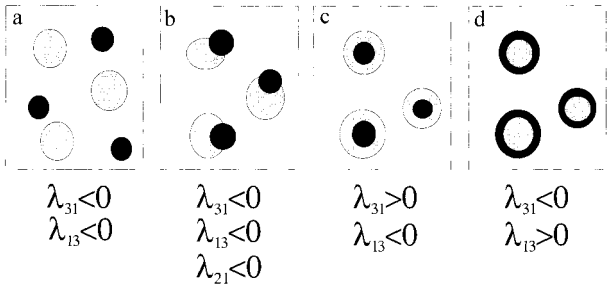

Figure 1. Schematic description of the different possible morphologies in a 1/2/3 ternary blend (black = phase 1; white = phase 2; grey = phase 3): (a) separate dispersions; (b) partial engulfing; (c) complete engulfing of phase 1 by phase 3; (d) complete engulfing of phase 3 by phase 1.

negative, a partial engulfing morphology could occur. These different cases are represented in Figure 1. In fact, this equation conveys, for a three-component system, the tendency for the particle which forms the highest interfacial tension with the matrix to enter within the other dispersed phase. They characterized the morphologies for a number of three- and four-component blends composed of various combinations of polystyrene (PS), bisphenol A polycarbonate (PC), poly(butylene terephthalate) (PBT), poly(methyl methacrylate) (PMMA) and poly(styrene-*co*-acrylonitrile) (SAN), thus possessing significantly different levels of interfacial interaction. The various morphologies which were formed and in particular the encapsulation effect, were in good agreement with those predicted from an analysis of spreading coefficients. Guo et al.[9] extended the spreading coefficient approach to take into account the overall surface free energy by including the interfacial area of each component. They report for different HDPE/PP/PS and HDPE/PMMA/PS immiscible polymer systems that the interfacial tension plays the major role in establishing the phase structure, whereas a less significant (but still important) role is played by the surface area of the dispersed phases, as determined by the composition. Although the above studies successfully demonstrated the usefulness of the spreading coefficient concept or surface free energy for understanding the formation of composite droplets, they do not discuss any strategies for selectively controlling which material forms the subinclusion phase.

Important studies were made concerning the controlled change of the phase structures of multiphase polymer blends from a classical matrix/dispersed phase system into a composite droplet system, or vice versa. Legros et al.[10] reported on a morphological study of poly(butylene terephthalate) (PBT)/polyethylene (PE)/ethylene vinyl acetate (EVA) ternary blends. This ternary system demonstrated very little subinclusion behavior. However, after addition of a transesterification precursor (Bu_2SnO) which is a selective interfacial modifier for PBT/EVA, the blend forms a composite droplet morphology. The formation of PBT/EVA copolymer, synthesized in situ, results in an EVA boundary layer between the incompatible PBT matrix and PE dispersed phase. This encapsulation is the result of a decrease in the EVA/PBT interfacial tension after compatibilization, leading to a much more positive EVA/PBT spreading coefficient. Guo et al.[9] showed the reverse effect and demonstrated that the phase structure of a HDPE/PP/PS ternary system (with HDPE as the matrix component) changed from a encapsulation type PP/PS to a separate droplet type by the addition to the blend system of a small amount of an interfacial modifier poly(styrene-*b*-ethylene) (S−E) block copolymer, i.e., by the reduction in PS/HDPE interfacial tension.

Even though the equilibrium morphology of composite droplets should in principle be determined by interfacial forces of thermodynamic origin, in practice this equilibrium morphology may not be achieved due to kinetic effects resulting from the high viscosities of polymers. Recent works have shown that both thermodynamic effects, expressed by means of spreading coefficient (or surface free energy), and kinetic effects, driven by the viscosities of the components, were found to affect the dispersed phase structure. Gupta and Srinivasan[11] studied ternary blends of isotactic polypropylene (PP), styrene−ethylene−butylene terpolymer (SEBS), and polycarbonate (PC) and correlated the melt rheological properties with the morphology of the dispersed phases. They found that the SEBS forms two types of morphologies depending on the blend composition and shear rate: simple droplets and a boundary layer at the surface of the PC droplets (with PP as the matrix). Nemirovski et al.[12] studied the phase morphology of a number of three-component systems. They show for a polypropylene (PP)/liquid crystalline polymer (LCP)/polystyrene (PS) blend that morphologies could be predicted when both thermodynamic and kinetic effects act cooperatively; i.e., spreading in ternary polymer blends should be enhanced by a low engulfing-to-engulfed phase viscosity ratio. They underline that careful attention should be paid when the effects are strongly opposing. In the case of a polypropylene (PP)/liquid crystalline polymer (LCP)/polycarbonate (PC) blend, in that same study, the very high viscosity of PC overcomes the weak thermodynamic driving force ($\lambda_{PC/LCP} = 0.16$) for encapsulation of LCP by PC. Thus, the kinetic effect, driven by the dispersed phase viscosity, can hinder the development of the expected structure, leading in practice to a sort of two-phase irregular PC/LCP domain and possibly an interpenetrating structure.

The purpose of this work is to examine the rapidity, stability and extent of subinclusion formation under dynamic mixing conditions. Factors influencing the internal structure as well as the size of the composite droplet will also be addressed. Both static and dynamic coalescence of these systems will be considered.

2. Experimental Procedure

2.1. Materials. Commercial HDPE, PS, and PMMA were examined in this study. The high-density polyethylene was 4352 N and the polystyrene was 615 APR, both obtained from Dow. The poly(methyl-methacrylate) pellets were IRD-2 obtained from Rohm & Haas. A small amount (0.2 wt %) Irganox B225 antioxidant from Ciba-Geigy was added to the mixture to reduce the thermal oxidation of polyethylene. Some of the characteristics of the resins are summarized in Table 1.

2.2. Rheological Analysis. Rheological characterization of the different homopolymers with 0.2 wt % antioxidant was carried out using a Rheometric Scientific constant stress rheometer (SR 5000) for PMMA and a Bohlin constant stress rheometer (CSM) for HDPE and PS. The experiments were performed in parallel-plate geometry with a gap of about 1.4 μm under a nitrogen atmosphere at a temperature of 200 °C. An oscillation mode at 0.1 Hz frequency was used to control the stability of the raw materials at 200 °C. A stress sweep was performed to define the region of linear viscoelasticity. We used the dynamic mode for high shear rates and the constant stress mode for low shear rates. They were used to determine the viscosity ratio of the blends used in this study.

Table 1. Material Characteristics

	M_w[a] × 10^{-3} (g/mol)	M_n[a] × 10^{-3} (g/mol)	melt index[b] (ASTM) (g/10 min)	density[b] (g/cm^3) at 20 °C	density[b] (g/cm^3) at 200 °C	η^* × 10^{-3} at 53 s^{-1} (Pa·s)	G' × 10^{-4} at 53 s^{-1} (Pa)	η_0 × 10^{-3} at 200 °C (Pa·s)
HDPE	79	24	4	0.962	0.754	0.95	2.4	1.4
PS	289.8	140.9	15	1.04	0.969	1.05	4.6	9.7
PMMA	76.5	46.8	5.5	1.19	1.0[c]	4.3	20.5	35.8

[a] Measured by GPC. [b] Obtained from suppliers. [c] At 230 °C.

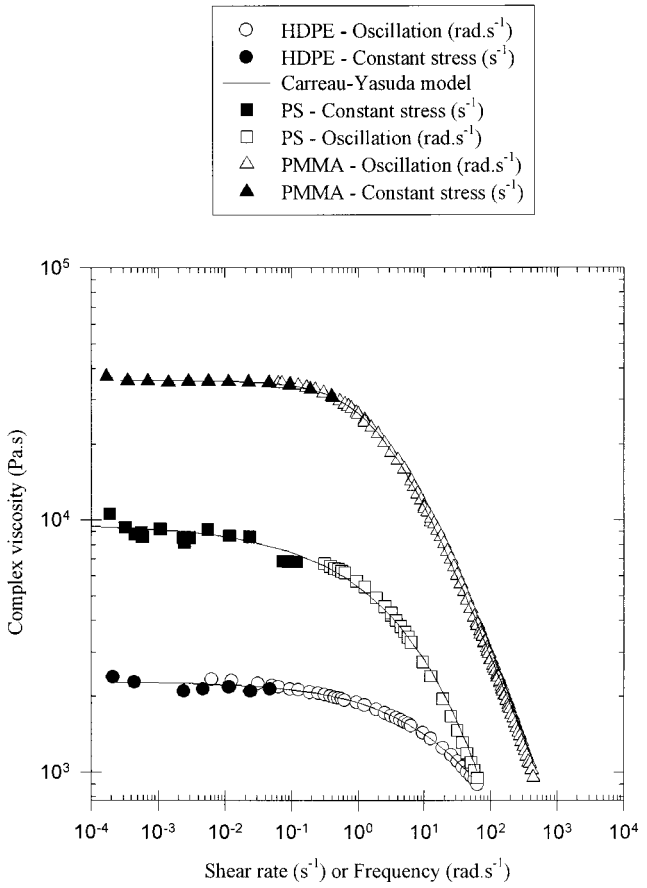

Figure 2. Complex viscosity as a function of the shear rate (s^{-1}) or frequency (rad·s^{-1}) at 200 °C for HDPE, PS and PMMA.

The zero shear viscosity obtained for the pure homopolymer was determined using a Carreau−Yasuda model. At low shear rates, the loss angle δ was sufficiently near 90° to consider the polymers as nonviscoelastic Newtonian fluids. It should be noted that the PMMA samples were dried 48 h under vacuum at about 70 °C to avoid bubble formation during the test. The rheological properties of the polymers are shown in Figure 2 and Table 1.

2.3. Breaking Thread Measurement. This well-known technique for the measurement of interfacial tension is based on the observation of capillary instability development. It consists of inserting a thread of one polymer between two films of the second polymer. Films were pressed from preblend resins between two metal plates on a Carver laboratory press at 200 °C. Fibers were obtained by drawing premixed pellets on a hot plate. The fiber diameters range from 10 to 80 μm. Threads were annealed for 24 h at a temperature slightly above the glass transition temperature to permit stress relaxation. This sandwich is then enclosed between two glass slides in a Mettler hot stage model FP 82-HT connected to a FP central processor. The observation of the samples was carried out on a Nikon transmission optical microscope. The sample is then brought to the desired temperature while care is taken that no pressure is exerted on the sample to avoid undesired deformation of the thread. Once the thread and the matrix have totally melted and relaxed, distortions start to grow and the change in amplitude is observed with time. To make these measurements, digitized images from the microscope were captured with a computer equipped by a Coreco Oculus image analysis system driven by Visilog 4.1.3 image analysis software. This software is able to record the time of the experiment while grabbing images. Measurements of the amplitudes and of the wavelengths were done by the software. Usually, two or three distortions were monitored per thread. Between 5 and 10 threads were monitored for each binary system. The typical error in the interfacial tension observed was ±10%. Details concerning the theoretical procedure for the measurements are reported elsewhere.[13,14]

2.4. Blend Preparation. Melt mixing was carried out in a 20 mL Brabender mixing chamber at 100 rpm. At this speed, the maximum shear rate in the mixing chamber is close to 53 s^{-1}. Pellets of the components and antioxidant were dry mixed before blending in the mixer. The mass of material charged into the mixer was chosen so that a constant volume of 20 cm^3 was achieved for each sample, based on the density at 200 °C. By definition, a time of mixing corresponds to the time between the start of feeding of the pellets into the mixer and the stopping of the roller blades. After mixing for the required time, the mixer drive was stopped and the front plate was removed, and samples were cut from the mass and dropped directly into a bath of cold water, to freeze in the morphology. The time required to feed the entire charge into the mixer varied from 18 to 25 s. It should be noted that all concentrations are reported as volume fraction.

2.5. Solvent Extraction. Selective solvent extractions of PS and PMMA in cyclohexane and acetic acid respectively were performed at room temperature during 1 week for the PS/PMMA blends over the whole composition range, to determine the point of phase inversion. Weight loss measurements were carried out to calculate the extent of co-continuity of PS (the same equation was used for PMMA) using the simple equation:

$$\% \text{ continuity} = \frac{(\text{weight PS}_{\text{init}} - \text{weight PS}_{\text{final}})}{\text{weight PS}_{\text{init}}} \times 100 \quad (2)$$

The maximum error is estimated at ±3 percent continuity units.

2.6. Morphological Analysis. Optical Microscopy. The polymer films used for the static coalescence study were prepared using the melt blended material pressed between two metal plates on a Carver laboratory press at 200 °C for 5 min. Optical observations of these polymer films were made using a Nikon transmission light microscope and photomicrographs were taken with a Nikon F601$_M$ camera. These experiments were carried out at high temperature (200 °C) using a Mettler FP-82HT hot stage controlled with a Mettler FP-90 central processor. The polymer film thickness was typically on the order of 100 μm.

Electron Microscopy. The specimens were microtomed under liquid nitrogen to create a plane face using a microtome (Leica−Jung RM 2065) equipped with a glass knife. The samples were also subjected to the appropriate chemical treatment during 48 h to selectively dissolve one of the minor phases. Cyclohexane and acetic acid were used to extract PS and PMMA respectively at room temperature. After coating the desired surface with a gold−palladium alloy for 14 min in pulse mode, morphological observations were carried out with a JEOL JSM 840 scanning electron microscope operated at a voltage of 10 or 15 kV.

Image Analysis. A semiautomatic method of image analysis consisting of a digitizing table and an in-house software was used to quantify the dispersed phase morphology. More

Table 2. Interfacial Tension for the Immiscible Binary Systems Obtained by the Breaking Thread Method at 200 °C

interface (thread/matrix)	σ (mN/m)
PS/HDPE	5.1
PMMA/PS	2.4
PMMA/HDPE	8.6

Table 3. Spreading Coefficients

polymer pairs	λ (mN/m)
PS/PMMA	1.1
PMMA/PS	−5.9
HDPE/PS	−11.3

than five fields of view and 900 diameters are considered for a given sample. The number-average diameter (D_n), the volume average diameter (D_v), and the surface fraction of the dispersed phase were obtained in this way. Since the microtome does not necessarily cut the dispersed phase spheres at the widest point, a correction was applied in order to obtain the true diameter and also to account for polydispersity effects.[15] The typical error for the measurement of D_v and D_n is about ±10%.

3. Results and Discussion

3.1. Viscosity Ratios, Interfacial Tensions, and Spreading Coefficients. Figure 2 shows the complex viscosity as a function of shear rate for the raw materials used. The viscosity of PS is higher than that of HDPE in the low shear rate region. At high shear rates and in particular in the region of shear rate corresponding to the estimated maximum shear rate during blending (53 s^{-1}), this effect is minimized with a PS/HDPE viscosity ratio of about 1.1. The PMMA is much more viscous than the other components for the whole range of shear rates. A high PMMA/HDPE viscosity ratio of 4.5 and a low PS/PMMA viscosity ratio of about 0.24 are observed in the region of estimated shear rate during blending.

The interfacial tension data listed in Table 2 were measured by the breaking thread method at 200 °C. The spreading coefficients were calculated from these interfacial tensions and are listed in Table 3. The spreading coefficient for the PS/PMMA pair is positive whereas the spreading coefficients for the PMMA/PS and HDPE/PS pairs are both negative. As has been discussed in the Introduction, this indicates that for ternary blends of HDPE/PS/PMMA with HDPE as the matrix phase, PMMA particles should be completely engulfed by the PS dispersed phase.

To confirm this assumption, the morphology of a HDPE/PS/PMMA 70/15/15 ternary blend at 2 min of mixing was investigated. The removal of the PS encapsulating phase by etching with cyclohexane is clearly apparent in Figure 3, parts a and c whereas the removal of the PMMA subinclusions by etching with acetic acid is observed in Figure 3, parts b and d. As might be expected, the morphology consists of a HDPE matrix, a nearly spherical PS encapsulating dispersed phase, and PMMA subinclusions within the PS dispersed phase.

3.2. Rapidity of Subinclusion Formation. The morphology development of a HDPE/PS/PMMA (70/15/15) blend mixed in an internal batch mixer as a function of the mixing time was investigated. The morphologies observed after 2 and 15 min of mixing are reported in Figure 3. First, the SEM photomicrographs in Figure 3, parts a and b clearly indicate, for this HDPE/PS/PMMA system, that the composite droplet morphology is obtained quite rapidly even when the time of mixing was only 2 min. We also observed a subinclusion morphology for a time of mixing of only 1 min but the samples were not homogeneous enough to be properly analyzed. It was pointed out earlier by Nemirovski et al.[12] that spreading in ternary polymer blends could also be enhanced by a low engulfing-to-engulfed phase viscosity ratio. Thus, if HDPE is chosen as the matrix, the low viscosity of the PS dispersed phase vs that of the PMMA (PS/PMMA viscosity ratio of about 0.24) would tend to favor the encapsulation of the PMMA by the PS phase rather the opposite. In this case, the kinetic effects due to the dispersed phase viscosity ratio act in the same direction as the thermodynamic considerations expressed by means of a positive $\lambda_{PS/PMMA}$ spreading coefficient. Second, if we compare the SEM photomicrographs at a mixing time of 2 and 15 min, the morphologies are very similar to each other. This is an indication that the time of mixing procedure does not affect the size or shape of the dispersed phase structure.

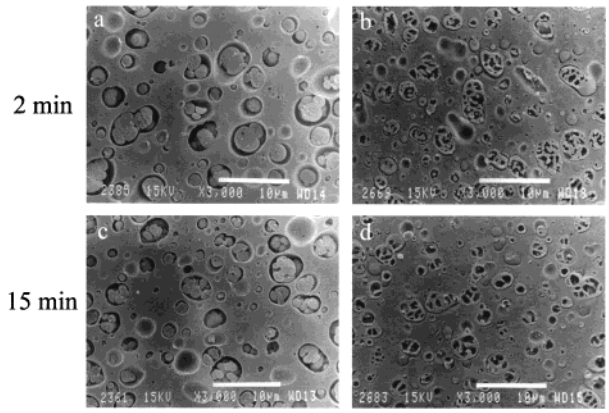

Figure 3. Dependence of the composite dispersed phase morphology on time of mixing. SEM photomicrograps of HDPE/PS/PMMA 70/15/15 ternary blend after extraction of the PS phase (left column) and the PMMA subinclusions (right column). The white bar denotes 10 μm.

Quantitative information is given in Figure 4, where the apparent size of the PS dispersed phase in the HDPE/PS/PMMA 70/15/15 ternary blend is plotted as a function of the mixing time. Increasing the mixing time from 2 to 15 min has little effect on the size of the composite dispersed phase considering that the typical error for the measurement of D_v is about ±10%. These results demonstrate not only the rapidity of the composite droplet morphology formation, but also the stability of this complex morphology. For comparison purposes, the results of the dependence of phase size on the time of mixing for a HDPE/PS 85/15 binary blend are also plotted in Figure 4. The constancy of the volume average diameter from 2 to 15 min of mixing is also observed in that case. These data are consistent with observations made by several authors reporting on the operation of internal mixers.[16−18] It was shown for immiscible blends that the most significant particle size deformation and disintegration processes took place within the first 2 min of mixing and that very little reduction in the size of the dispersed phase was observed thereafter. Macosko et al.[19] studied the evolution of the average diameter of PMMA/PS blends both with and without symmetric poly(S-*b*-MMA) diblock copolymers as a function of the mixing residence time; 3 and 8 min of mixing respectively (at a maximum shear rate of about 50 s^{-1}) was required to reach the final

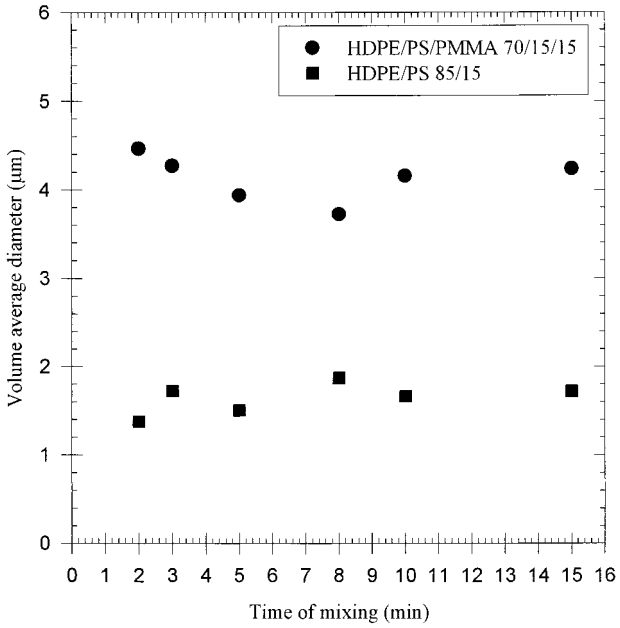

Figure 4. Dispersed phase diameter as a function of mixing time for HDPE/PS/PMMA 70/15/15 and HDPE/PS 85/15.

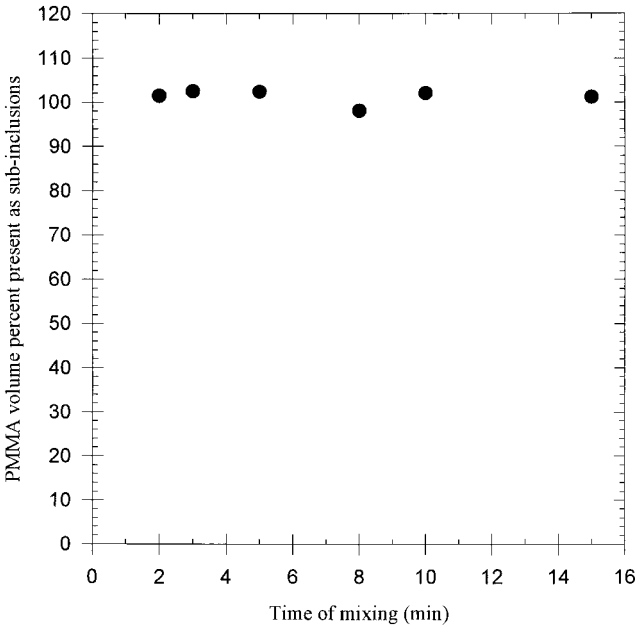

Figure 5. Volume percent PMMA effectively present as subinclusions within the PS dispersed phase as a function of the mixing time for the HDPE/PS/PMMA 70/15/15 ternary blend.

particle size. The present work is the first quantitative time of mixing study for a ternary blend which forms subinclusion morphologies. However, such results were not observed by Nemirovski et al.[12] for a polypropylene (PP)/liquid crystalline polymer (LCP)/polystyrene (PS) 76.5/13.5/10 (wt %) ternary blend in their qualitative study on subinclusion morphology. They showed an evolution in the dispersed phase morphology with the time of mixing: At 4 min of mixing, they observed LCP particles with a low coverage of PS. At 6 min of mixing, LCP domains were engulfed by a PS shell that was drawn from a larger PS region, while other LCP particles were in the process of being coated by the spreading PS layer. Finally, this led to the complete engulfing of LCP domains by the PS after 15 min of mixing. It should be noted that in their work, the viscosity of the PS layer is greater than the viscosity of the LCP by a factor 3. This represents an opposing kinetic effect to the development of subinclusions. Even though it is not enough strong to hinder formation of the composite droplet morphology, the kinetic effect is sufficiently strong to delay the encapsulation phenomena.

3.3. Extent of Subinclusion Formation. One of the main questions to be answered concerning composite droplet formation is to determine to what extent or degree the PS finds its way to the interface between the HDPE and the PMMA in the melt mixing process. From a careful visual analysis of Figure 3, parts b and d (PMMA etching), it appears that all the PMMA phase is present as subinclusions within the PS dispersed phase and none exists as a discrete dispersed phase. To confirm this visual assessment, calculation of the PMMA volume percent effectively present as subinclusions is performed via measurements of the PS apparent surface fraction, assuming that the measured surface fraction is equal to the volume surface fraction. If PMMA subinclusions exists within the PS dispersed phase, the PS surface fraction measured after cyclohexane etching should increase since both the dispersed PS and PMMA subinclusions are extracted out. The PMMA volume percent present as a discrete dispersed phase in a HDPE/PS/PMMA 70/15/15 ternary blend can then be defined as the PS surface percentage measured in the HDPE/PS 70/30 binary blend minus the PS "apparent" surface percentage obtained in the HDPE/PS/PMMA 70/15/15 ternary blend. The values are compared for an equal total amount of dispersed phase. Thus, a difference of 0% in the measured PS surface corresponds to the case where the 15% PMMA of the HDPE/PS/PMMA 70/15/15 blend is completely within the PS dispersed phase, i.e., 100% of PMMA is present as subinclusions in the PS dispersed phase. At the opposite end, a difference of 15% in the apparent PS surface area represents the case where 0% PMMA is present as subinclusions i.e., PS and PMMA are dispersed as discrete particles. This calculation assumes that the PS/PMMA interface contains no microvoids which could distort the measurements of the PS apparent surface fraction. This assumption has been confirmed by microscopic observations.

The results obtained for a 70/15/15 HDPE/PS/PMMA ternary system are reported in Figure 5 as a function of the mixing time. The average error in the calculation of PMMA volume percent effectively present as subinclusions is estimated at about ±10%. The constancy of this function around 100% indicates clearly that for this composition, all the PMMA is present as subinclusions within the PS dispersed phase even when the time of mixing is only 2 min. Furthermore, the quantity of subinclusions remains stable thereafter, showing that PMMA subinclusions result from a stable process.

Measurements were made for HDPE/PS/PMMA ternary blends with a constant content of the major component (HDPE; 80 vol %) but with various PS/PMMA composition ratios. The time of mixing is kept constant at 8 min and is sufficiently long to attain a quasi-equilibrium or steady-state morphology (see Figure 4 as a demonstration). Figure 6 plots the PMMA volume percent effectively present as subinclusions in the composite dispersed phase as a function of the PS content in the dispersed phase. Taking into account the

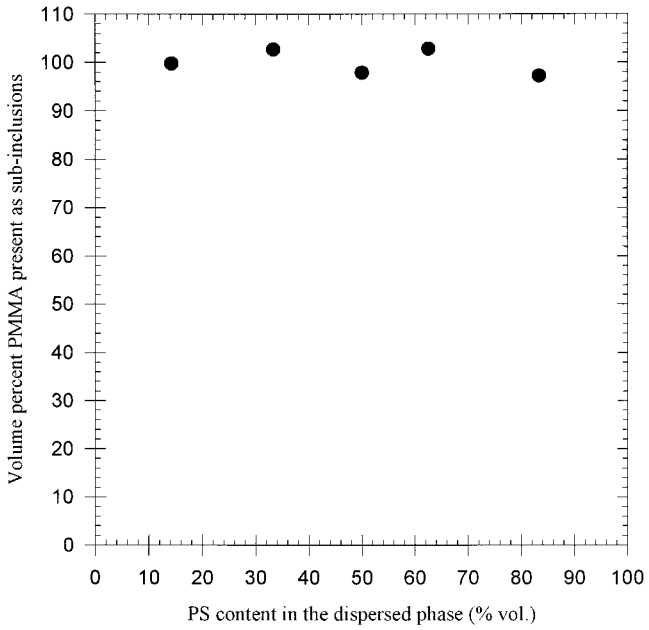

Figure 6. Volume percent PMMA effectively present as subinclusions within the PS dispersed phase as a function of the PS content in the dispersed phase for the 80(HDPE)/20(PS + PMMA).

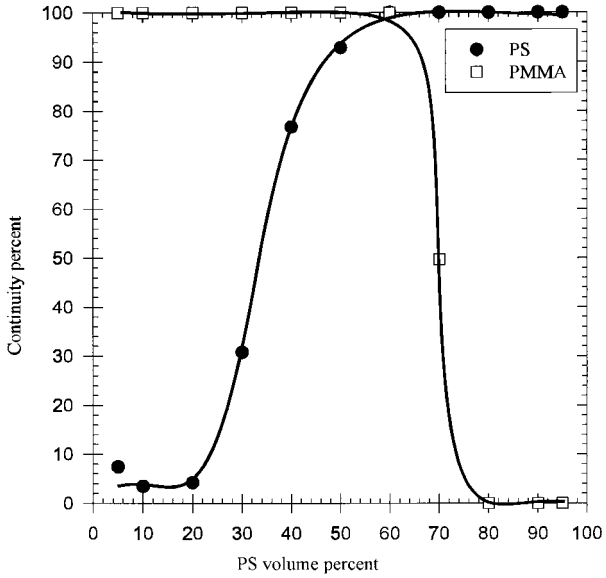

Figure 7. Degree of phase continuity vs composition for the PS/PMMA blend.

average error in the calculation of this volume percent, it can be said that effectively all the PMMA is present as subinclusions within the PS dispersed phase over the entire PS/PMMA composition range.

Conceptually, the formation of the subinclusion morphology is a similar process to the interfacial modification of immiscible binary blends. A calculation of the surface energy reduction associated with the composite droplet structure (vs separate dispersed phases) can be compared to the interfacial energy reduction associated with the compatibilization of different binary systems.[20−22] This is estimated using the surface area of dispersed phase and the interfacial tension before and after each process. The results indicate a similar value on the order of 1000 J/m^3. Recently, Cigana and Favis[23] have demonstrated that all the modifier goes to the interface in a PS/EPR blend. The results of this study appear to support that conclusion. The question of surface energy reduction will be discussed in more detail in a following study.

3.4. Manipulation of the Dispersed Phase Internal Structure. Recent studies have shown that the ultimate mechanical properties of multiphase polymer blends of more than two phases are greatly influenced by their phase morphologies.[24,25] One of the main parameters controlling the composite droplet microstructure is the composition. In this section, a constant content of the major component (HDPE; 80 vol %) is maintained and the volume ratio of the two minor constitutive components (PS/PMMA) is changed extensively. To understand the phase size/composition relationship for PS and PMMA, binary blends were prepared. Selective solvent extraction of the PS and PMMA phases allows for the identification of the region of phase inversion (see Figure 7). The region of phase inversion occurs at about 60%.

Figure 8 illustrates the systematic evolution of the internal microstructure of the dispersed phase with decreasing PS/PMMA ratio (from left to right). One can observe that whatever the PMMA content, it systematically forms a subinclusion structure in the PS phase, as expected by calculation of the spreading coefficients.

For a high content of PS (Figure 8a), the phase morphology formed by the two minor components is constituted of distinct particles of PMMA dispersed in a larger (and thus continuous) phase of PS. These distinct particles coalesce and increase in size with increasing PMMA content (Figure 8b), as is observed in a binary polymer blend. When sufficient PMMA is added to provoke binary blend phase inversion as observed in Figure 7 (< 60% of PS content), a particular effect is observed. The PMMA subinclusions cannot go to the outside to become the continuous phase because of the opposing thermodynamic driving forces. Further increasing the PMMA content beyond the phase inversion leads to a complete core−shell structure with occasional ligaments spanning across the particle (Figure 8c) due to incomplete coalescence (also see Figure 10c). This is a clear indication that thermodynamic forces are strong enough to prevent the phase inversion process. Further increasing the PMMA concentration leads to the appearance of PS particles of the shell material in the PMMA phase (Figure 8d). These observations are consistent with previous work by Luzinov et al.[25] for a PS/SBR/PE ternary system. They observed a PS matrix, SBR shell, and SBR particles within the PE core. They suggest that this is due to the tendency of PE to envelop SBR at PE contents larger than the theoretical phase inversion point. In that case an impeded phase inversion process is not unexpected since the SBR copolymer possesses segments that are miscible with each component. The SBR acts as a classic interfacial modifier interpenetrating each phase and acting as an adhesion promoter between the phases. In the present case where interfacial tensions between the phases are substantially higher and very little intermixing is expected between the phases, the thermodynamic driving forces are still strong enough to prevent phase inversion.

Another important question remaining is: what is the smallest possible shell that can be obtained? Is it possible to obtain molecular dimensions? In this study, a complete coverage is observed at 14% of PS (based on

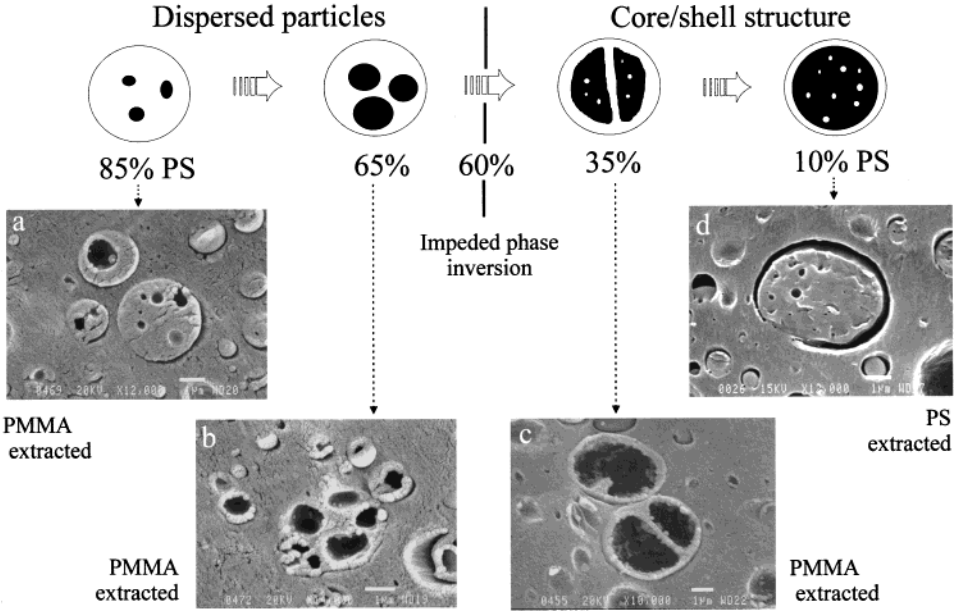

Figure 8. Evolution of the dispersed phase internal structure as a function of the PS content (Vol.% in the dispersed phase) for the 80 (HDPE)/20 (PS + PMMA) ternary blend.

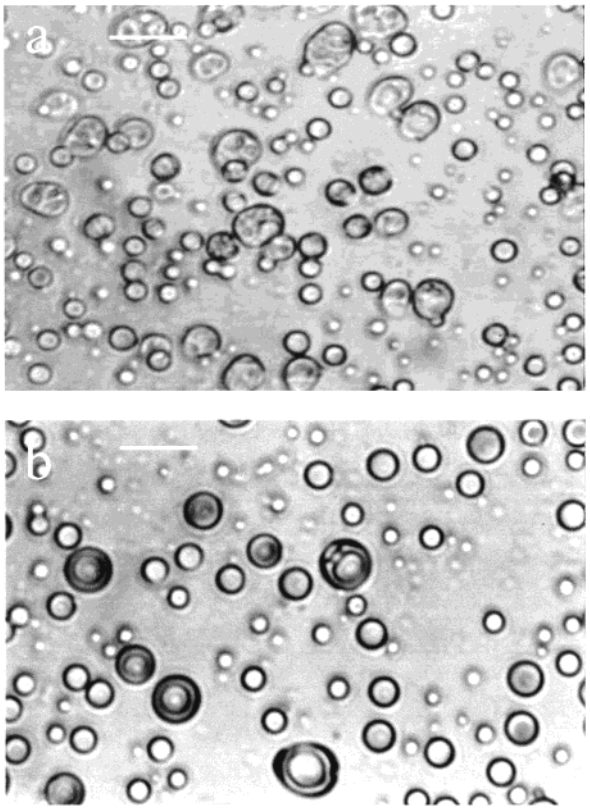

Figure 9. Effect of annealing time on morphology for HDPE/PS/PMMA 90/5/5 ternary blend: (a) 2 min; (b) 90 min. The white bars denote 10 μm.

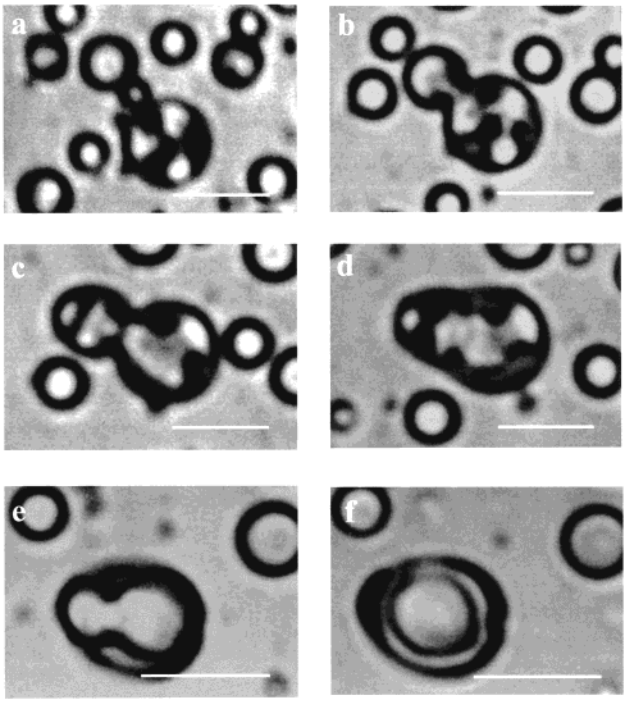

Figure 10. Static coalescence between composite droplets for HDPE/PS/PMMA 90/5/5 ternary blend as a function of the annealing time: (a) 2 min; (b) 9 min; (c) 17 min; (d) 28 min; (e) 60 min; (f) 90 min. The white bars denote 10 μm.

the dispersed phase) and it appears that there is partial coverage at lower PS content.

3.5. Coalescence of Composite Droplet Dispersed Phase. The coalescence process is critical to controlling polymer blend morphology, and to date the observation of composite droplet coalescence has not been performed or studied. A number of questions need to be asked. Does the composite droplet coalesce in "classic fashion" as the binary blend? Does coalescence diminish when a low interfacial tension shell encapsulates the subinclusion material? Is the internal structure sensitive to coalescence? What is the interplay between dispersed phase and subinclusion coalescence?

Static Coalescence. A thin film of a HDPE/PS/PMMA 90/5/5 ternary blend was examined by annealing at 200 °C. By definition, a time of annealing corresponds to the time between the start of microscopic observations after the compression molding stage and the time when the picture was taken. Parts a and b of Figure 9 illustrate the morphology observed at 2 and 90 min of annealing, respectively. The presence of the composite multiphase morphology is clearly observed in Figure 9a. We can also infer from this photomicrograph that the

predominant phase morphology formed by the two minor components is one of dispersed particles of PMMA in a PS shell. Figure 9b demonstrates the complete transition to a core−shell PMMA/PS structure after 90 min of annealing time.

Photomicrographs for different periods of annealing times going from 2 to 90 min regrouped in Figure 10 allows one to observe the coalescence process of composite droplets. Figure 10a displays three composite droplet particles in contact with each other. The largest particle is clearly composed of three separate subinclusions in a PS shell. When the annealing time is increased from 2 to 9 min (Figure 10b), core−core and shell-shell coalescence is clearly shown to be taking place. Note the presence of a new composite droplet coming into contact with the others in the upper left-hand corner, the shells are just touching. In Figure 10c, a significant degree of shell−shell coalescence has taken place for the latter particle. As one progresses from Figure 10b to Figure 10f, it can be seen that the four or five initial composite droplet particles coalesce into a stable, spherical, and well-defined core−shell morphology.

It can be concluded that the coalescence process observed in binary blends is also observed in ternary blends. Composite droplets clearly experience a dual coalescence process, first between PMMA subinclusions within composite droplets, and second between composite droplets themselves. Although some particle size increase is visually observed, the main effect of static coalescence in this study is on the internal structure of the dispersed phase at long times of annealing treatment. The initial discrete PMMA subinclusions in PS tend to coalesce, thus resulting in a core−shell structure. This effect can reasonably be expected to depend on the composition of the various components. In this case, the composite droplet is present at a concentration of only 10% with respect to the matrix, while the composite droplet itself is a PS/PMMA 50/50 blend. Lowering the composition of subinclusions in the dispersed phase should significantly hinder the transition to a core−shell morphology. Note as well that the transition from dispersed subinclusions to a core−shell structure is taking place under the difficult condition of a highly viscous PMMA and low PS/PMMA interfacial tension. Presumably other ternary systems carried out under similar conditions to this experiment could form the core−shell morphology much more rapidly.

Dynamic Coalescence. Even though the photomicrographs reported in Figure 9 and Figure 10 provide direct evidence that coalescence can occur both between the composite droplets and between subinclusions upon annealing, what is the impact of subinclusions in the dispersed phase on coalescence under dynamic conditions?

It has been shown in a recent work that a low interfacial tension PVC/LLDPE blend revealed virtually no change in particle size with composition.[21] This blend therefore does not experience significant dynamic coalescence phenomena during melt mixing. In the same way, the presence of an interfacial agent in a binary blend leads to a decrease of the particle size with composition, again due to the prevention of coalescence through immobilization of the interface and reduction of the interfacial tension.[22] In this study coalescence effects under dynamic mixing conditions are examined by considering the dispersed particle size/composition

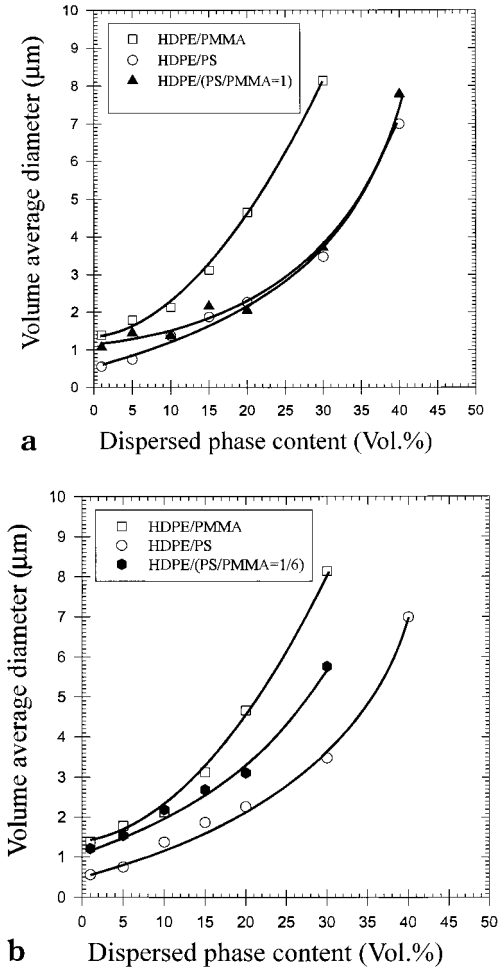

Figure 11. (a) Dispersed phase diameter as a function of the dispersed phase content for HDPE/PS/PMMA ternary blends where PS/PMMA = 1. Comparison with HDPE/PS and HDPE/PMMA binary blends. In all cases HDPE is the matrix. (b) Dispersed phase diameter as a function of the dispersed phase content for HDPE/PS/PMMA ternary blends where PS/PMMA = $^1/_6$. Comparison with HDPE/PS and HDPE/PMMA binary blends. In all cases HDPE is the matrix.

relationship. The evolution of the diameter with composition for HDPE/PS/PMMA ternary blends with a constant PS/PMMA composition ratio equal to 50/50 is plotted in Figure 11a. A direct conclusion arising from this curve is that dynamic coalescence occurs for the composite droplet morphology since the volume average diameter increases with composition. Furthermore, the respective binary blends, HDPE/PS and HDPE/PMMA, studied as reference systems, yield interesting information. Despite the high viscosity of the PMMA subinclusions, the curve for the ternary blend is almost similar to that of the HDPE/PS blend, except at low contents of dispersed phase where its behavior is closer to that of the HDPE/PMMA blend. These results indicate that if the outer shell is thick enough, the dispersed phase coalescence process depends much more on the interfacial and viscoelastic properties of the external layer than that of the subinclusions. For a constant PS/PMMA composition ratio, the PS shell thickness decreases with decreasing dispersed phase content. Below a critical value corresponding roughly to 20% dispersed phase in Figure 11a, the PMMA begins to dominate the coalescence process. It needs to be confirmed whether this is due to incomplete coverage or simply the thickness of the shell.

With simple geometrical arguments, it is possible to derive an expression to describe the PS shell thickness for the case of dispersed spherical particles. If D_v is the volume average diameter of composite droplet particles, and ϕ_v the volume fraction of PS (based on the dispersed phase), then the PS shell thickness H is given by

$$H = \frac{1}{2} D_v[1 - \sqrt[3]{(1 - \phi_v)}] \quad (3)$$

It must be pointed out that in carrying out this analysis for a ternary blend, one has to assume that all the PS phase is situated at the interface and that the PMMA phase is only present as subinclusions. Previous work reported earlier in this paper indicates that these are reasonable assumptions. We also assume no multicore structures but only a core−shell morphology. In this way, the calculated value of the shell thickness corresponding to 20% dispersed phase is about 0.2 μm.

To confirm the effect of shell thickness on droplet size formation, an experiment was also designed at low PS concentration. The evolution of the diameter with composition at a PS/PMMA composition ratio equal to $^1/_6$ is presented in Figure 11b and shows that its behavior at low dispersed phase concentration is very close to that of the HDPE/PMMA binary blend. A definite tendency to move toward the HDPE/PS curve is observed at higher dispersed phase concentration. In this case, however, the HDPE/PS composition curve is not attained even at a high content of dispersed phase. The estimated PS shell thickness calculated for 30% dispersed phase is 0.14 μm. That value is below the critical shell thickness obtained for the 80% HDPE/20% (PS/PMMA = 1) ternary blend.

3.6. Control of the Composite Droplet Size. Because of the importance of controlling the dispersed phase size in polymer blends, attention was given to the relationship between the PS/PMMA composition ratio and the composite droplet size. In section 3.5 the composite droplet particle size as a function of dispersed phase content was studied at two PS/PMMA compositions. In this part, the volume average diameter D_v of the composite dispersed phase is plotted vs a wide range of PS content at a fixed dispersed phase content of 20%. The results are represented in Figure 12. The composite droplet particle size decreases from 4.6 to about 2 μm as the quantity of PS is increased from 0% to 50% (based on the dispersed phase content). Further increasing the quantity of PS above 50% did not significantly change the particle size. Furthermore, the 80/20 HDPE/PMMA binary blend exhibits relatively wide polydispersity ($D_v/D_n = 3.6$) because of the high viscosity ratio between the HDPE matrix and the PMMA dispersed phase, whereas increasing the concentration of PS up to a 50/50 PS/PMMA leads to a decrease of the composite droplet size polydispersity ($D_v/D_n = 2.6$).

The curve in Figure 12 has the typical shape of an emulsification curve as described by Cigana et al.[26] and Willis and Favis[27] for compatibilized binary systems. They report the sharp reduction in the minor phase size upon addition of small amounts of interfacial agent, followed by a leveling-off at higher concentration. The lowering of the dispersed phase size in that case is explained in terms of interfacial tension and coalescence reduction. Furthermore, the concentration at which equilibrium is reached in those studies corresponds to the saturation of the interface by the interfacial agent (generally at about 5−20 wt % of interfacial modifier

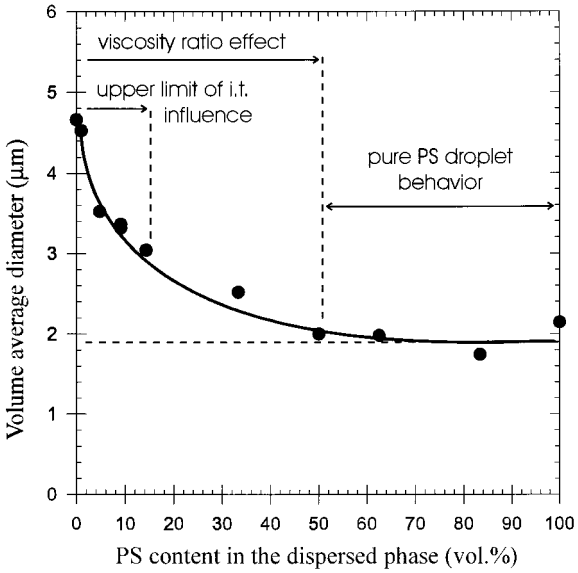

Figure 12. Dispersed phase size as a function of PS content in the dispersed phase for the 80(HDPE)/20(PS + PMMA) ternary blend.

based on the dispersed phase). In this study on composite droplets one can also envisage a quasi-emulsifying effect played by the PS, and postulate that the presence of a PS layer at the interface between the HDPE matrix and the PMMA dispersed phase decreases interfacial tension and perhaps also coalescence.

To better understand the role played by the PS layer on the composite droplet size, compare the average diameter of the 80/20 HDPE/PMMA binary blend and the 80% HDPE/20% (PS + PMMA) ternary blend at 50% of PS (based on the dispersed phase volume) with the decrease of interfacial tension from $\sigma_{HDPE/PMMA}$ to $\sigma_{HDPE/PS}$. An overall decrease of about 2.5 times in the volume average diameter was observed at a PS content of 50% whereas a 1.7-fold reduction in interfacial tension is estimated. The lowest PS concentration at which we can confirm complete encapsulation is at 14% PS. That value therefore represents the upper limit of complete encapsulation of the PMMA phase by PS, and hence the full effect of interfacial tension on particle size reduction should be accomplished by that point. What is the reason for the continued decrease in particle size from 14% up to 50% PS?

As the PS percent increases, the shell thickness also increases, and this changes the rheological properties of the droplets. In fact, depending on the composition of the dispersed phase, the composite droplet experiences a viscosity ratio with the HDPE matrix which varies from 4.5 (PMMA/HDPE) to 1.1 (PS/HDPE). A lower viscosity ratio results in a smaller particle size.[5]

Figure 12 also provides evidence that the addition of a volume of 50% or more of PS subinclusions has little further effect on the composite droplet particle size. Apparently, there exists a critical shell thickness value above which the composite droplet behaves microrheologically as pure shell material during the melt mixing process. Using eq 3 to calculate the PS shell thickness corresponding to 50% PS, a shell thickness of 0.2 μm is obtained. This value is very similar to the critical shell thickness reported in the *coalescence* part where, above a shell thickness of about 0.2 μm, the system demonstrated coalescence behavior identical to pure PS. These independent results reinforce the concept of a critical shell thickness.

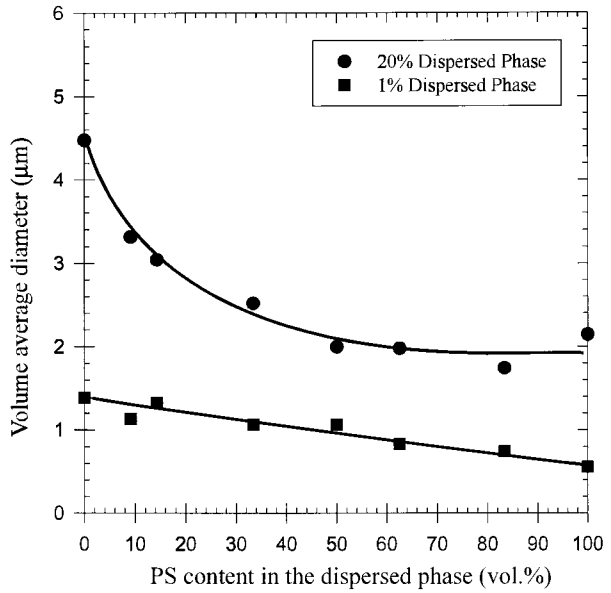

Figure 13. Dispersed phase size as a function of PS content in the dispersed phase for the 99(HDPE)/1(PS + PMMA) and the 80(HDPE)/20(PS + PMMA) ternary blends.

Recent work from this group demonstrated a linear relationship between the drop in dispersed phase size and the interfacial tension reduction in the absence of coalescence.[20,21] It is interesting to note that at 14% PS, a system where PMMA is completely encapsulated by PS, the reduction in particle size as compared to HDPE/PMMA is 1.6. This is similar to the 1.7 times decrease in interfacial tension from a HDPE/PMMA to a HDPE/PS interface. Thus, up to 14% PS, the reduction in composite droplet diameter is dominated by an interfacial tension reduction.

The results therefore indicate that at low PS content (up to 14%), the particle size reduction is strongly influenced by interfacial tension reduction. The low viscosity of the PS shell influences particle size reduction up to 50% PS. Beyond 50% PS, in excess of a critical shell thickness of 0.2 μm, the composite droplet particle behaves as pure PS.

To confirm the effect of shell thickness on droplet size formation, an experiment was also designed at a lower fixed dispersed phase content. The evolution of the diameter with PS/PMMA composition ratio at a fixed dispersed phase content of 1% is presented in Figure 13. Its behavior is different to that of the fixed dispersed phase content of 20% also shown in Figure 13. Clearly, the composite droplet particle size decreases in a monotonic fashion from 1.4 to about 0.6 μm as the quantity of PS is increased from 0% to 100% (based on the dispersed phase content). In the case of the 1% dispersed phase content, the particle size curve never reaches a plateau even at a high content of PS. The estimated PS shell thickness at 84% PS content is 0.18 μm. That value is still below the 0.2 μm critical shell thickness obtained for the 80% HDPE/20% (PS/PMMA) ternary blend.

4. Conclusion

This work demonstrates for HDPE/PS/PMMA ternary blends, that the encapsulation process occurs very early in the compounding operation and remains stable in time. The morphology observed is composed of a HDPE matrix, a PS dispersed phase, and PMMA subinclusions within the PS dispersed phase. Furthermore, it was shown quantitatively that all the PMMA is present as subinclusions within the PS dispersed phase. Control of the composite droplet morphology can be achieved by altering the relative proportion of PS and PMMA. Thus, it is possible to manipulate the dispersed phase internal structure from small PMMA subinclusions dispersed in a larger PS particle to a PS/PMMA core−shell structure upon decreasing the PS/PMMA ratio. This core−shell structure is the result of an impeded phase inversion phenomena.

It was also found that the coalescence process observed in binary blends is also observed in these ternary blends. Composite droplets clearly experience a dual-coalescence process: (a) between subinclusions and (b) between composite droplets. A complete transition from multiple subinclusion particles within a given shell to a core−shell structure was observed upon annealing. Furthermore, it is clearly shown that coalescence also occurs under dynamic mixing conditions, since the composite droplet size increases with composition. It is demonstrated that the coalescence behavior of the composite droplet is essentially equal to that of a pure PS dispersed phase above a critical PS shell thickness of about 0.2 μm.

In particular, the study of the composite droplet size for the 80% HDPE/20% (PS + PMMA) shows that increasing the PS content leads to a significant composite droplet particle size reduction. This is related to the presence of the PS shell at the HDPE/PMMA interface, which lowers the interfacial tension and also reduces the matrix/dispersed phase viscosity ratio with increasing shell thickness. These results also indicate that the composite droplet size resulting from breakup and coalescence is independent of the PS/PMMA ratio once a PS critical shell thickness of 0.2 μm is achieved. Above that thickness the composite droplet behaves in a fashion similar to a pure PS droplet.

References and Notes

(1) Amos, J. L.; McIntyre, O. R.; Mc Curdy, J. L. U.S. Patent 1954, 2 694 692.
(2) Molau, G. E.; Keskula, H. *J. Polym. Sci.* **1966**, *4*, 1595.
(3) Berger, W.; Kammer, H. W.; Kummerlöwe, C. *Makromol. Chem.* **1984**, *Suppl. 8*, 101.
(4) Van Oene, H. *J. Colloid Interface Sci.* **1972**, *40*, 448.
(5) Favis, B. D.; Chalifoux, J. P. *Polymer* **1988**, *29*, 1761.
(6) Favis, B. D.; Lavallée, C.; Derdouri, A. *J. Mater. Sci.* **1992**, *27*, 4211.
(7) Torza, S.; Mason S. G. *Colloid Sci.* **1970**, *33*, 67.
(8) Hobbs, S. Y.; Dekkers, M. E. J.; Watkins, W. H. *J. Mater. Sci.* **1988**, *23*, 1219.
(9) Guo, H. F.; Packirisamy, S.; Gvozdic, N. V.; Meier, D. J. *Polymer* **1997**, *38*, 785.
(10) Legros, A.; Favis, B. D.; Carreau, P.; Michel, A. *Polymer* **1997**, *38*, 5085.
(11) Gupta, A. K.; Srinivasan, K. R. *J. Appl. Polym. Sci.* **1993**, *47*, 167.
(12) Nemiroski, N.; Siegmann, A.; Narkis, M. *J. Macromol. Sci.—Phys.* **1995**, *B34*, 459.
(13) Elemans, P. H. M, Janssen, J. M. H.; Meijer, H. E. H. *J. Rheol.* **1990**, *34*, 1311.
(14) Tomotika, S. *Proc. R. Soc. London, Ser. A* **1935**, *A150*, 322.
(15) Saltikov, S. A. *Proceedings of the 2nd International Congress for Stereology*, Helias: New York, 1967.
(16) Schreiber, H. P.; Olguin, A. *Polym. Eng. Sci.* **1983**, *23*, 129.
(17) Karger-Kocsis, J.; Kallò, A.; Kuleznev, V. N. *Polymer* **1984**, *25*, 279.
(18) Favis, B. D. *J. Appl. Polym. Sci.* **1990**, *39*, 285.
(19) Macosko, C. W.; Guegan, P.; Khandpur, A. K.; Nakayama, A.; Marechal, P.; Inoue, T. *Macromolecules* **1996**, *29*, 5590.

(20) Lepers, J. C.; Favis, B. D.; Tabar, R. J. *J. Polym. Sci., Part B: Polym. Phys.* **1997**, *35*, 2271.
(21) Liang, H.; Favis, B. D. *Macromolecules* **1999**, *32*, 1637.
(22) Mekhilef, N.; Favis, B. D.; Carreau, P. *J. Polym. Sci.: Part B: Polym. Phys.* **1997**, *35*, 293.
(23) Cigana, P.; Favis, B. D. *Polymer* **1998**, *39*, 3373.
(24) Guo, H. F.; Gvozdic, N. V.; Meier, D. J. *PMSE Prepr.* **1996**, *75*, 444.
(25) Luzinov, I.; Xi, K.; Pagnoulle, C.; Huynh-Ba, G.; Jérôme, R. *Polymer* **1999**, *40*, 2511.
(26) Cigana, P.; Favis, B. D.; Jérôme, R. *J. Polym. Sci., Part B: Polym. Phys.* **1996**, *34*, 1691.
(27) Willis, J. M.; Favis, B. D. *Polym. Eng. Sci.* **1988**, *28*, 1416.

MA991954G